Earth and Planetary Science Letters 298 (2010) 347–360

Contents lists available at ScienceDirect

Earth and Planetary Science Letters

journal homepage: www.elsevier.com/locate/epsl

Strain accumulation across the Messina Straits and kinematics of Sicily and Calabria from GPS data and dislocation modeling

E. Serpelloni [a,*], R. Bürgmann [b], M. Anzidei [a], P. Baldi [c], B. Mastrolembo Ventura [c,d], E. Boschi [a,c]

[a] Istituto Nazionale di Geofisica e Vulcanologia, Centro Nazionale Terremoti, Italy
[b] Department of Earth and Planetary Science, University of California, Berkeley, CA, USA
[c] Department of Physics, University of Bologna, Italy
[d] Istituto Nazionale di Geofisica e Vulcanologia, Sezione di Bologna, Italy

ARTICLE INFO

Article history:
Received 1 December 2009
Received in revised form 31 July 2010
Accepted 6 August 2010
Available online 9 September 2010

Editor: R.D. van der Hilst

Keywords:
Messina Straits
Global Positioning System
strain accumulation
plate kinematics
dislocation modeling

ABSTRACT

We use Global Positioning System (GPS) velocities and dislocation modeling to investigate the rate and nature of interseismic strain accumulation in the area affected by the 1908 Mw 7.1 Messina earthquake (southern Italy) within the framework of the complex central Mediterranean microplate kinematics. Our data confirm a change in the velocity trends between Sicily and Calabria, moving from NNW-ward to NE-ward with respect to Eurasia, and detail a fan-like pattern across the Messina Straits where maximum extensional strain rates are ~65 nanostrains/yr. Extension normal to the coast of northern Sicily is consistent with the presence of SW–NE trending normal faults. Half-space dislocation models of the GPS velocities are used to infer the slip-rates and geometric fault parameters of the fault zone that ruptured in the Messina earthquake. The inversion, and the bootstrap analysis of model uncertainties, finds optimal values of $3.5^{+1.3}_{-2.0}$ and $1.6^{+0.2}_{-0.3}$ mm/yr for the dip–slip and strike–slip components, respectively, along a $30^{+0.7°}_{-1.1}$ SE-ward dipping normal fault, locked above $7.6^{+2.9}_{-4.6}$ km depth. By developing a regional elastic block model that accounts for both crustal block rotations and strain loading at block-bounding faults, and adopting two different competing models for the Ionian–Calabria convergence rates, we show that the measured velocity gradient across the Messina Straits may be significantly affected by the elastic strain contribution from other nearby faults. In particular, when considering the contribution of the possibly locked Calabrian subduction interface onto the observed velocity gradients in NE-Sicily and western Calabria, we find that this longer wavelength signal can be presently super-imposed on the observed velocity gradients in NE-Sicily and Calabria. The inferred slip-rate on the Messina Fault is significantly impacted by elastic strain from the subduction thrust. By varying the locking of the subduction thrust fault, in fact, the Messina Fault slip-rate varies from 0 to 9 mm/yr.

1. Introduction

The Messina Straits (Southern Italy), a narrow basin structure located between the Calabrian and Sicilian coasts (Fig. 1), and traditionally interpreted as a recent rift zone characterized by graben-style faulting (Ghisetti, 1984), was the locus of one of the strongest seismic events that ever hit Italy during historical times, the M_w 7.1 December 28, 1908 Messina–Reggio Calabria earthquake. The same area also suffered major damage from other earthquakes of comparable magnitude in the last few centuries, such as the southern Calabria earthquake of February 5, 1783 (Boschi et al., 2000).

While a general consensus indicating normal-faulting as the dominant mechanism for the 1908 earthquake has been reached, the exact location and geometry of its causative fault are still controversial (Amoruso et al., 2002; Bottari et al., 1989; Ghisetti, 1984; Monaco and Tortorici, 2000; Pino et al., 2009; Valensise and Pantosti, 1992). Furthermore, little is known about the shape and rate of interseismic strain across the Messina Straits. Even though this region has been surveyed since the early 1970s by means of terrestrial techniques (Anzidei et al., 1998; Bencini, 1975; Caputo et al., 1981), evidence of active deformation remained elusive until more recent times. Hollenstein et al. (2003) analyzed epoch GPS (EGPS) measurements, carried out between 1994 and 2001, but found no significant deformation across the Straits. D'Agostino and Selvaggi (2004) and Serpelloni et al. (2005), by combining EGPS and continuous GPS (CGPS) observations, found a significant NW–SE extension, with values of up to 3 mm/yr. More recently, Mattia et al. (2009) found ~150 nanostrains/yr of extension in NE-Sicily, with a highly variable pattern of principal strain-rate orientations across the Straits.

To improve our knowledge of crustal deformation and microplate kinematics in the study area we take advantage of recent advances of

* Corresponding author. Istituto Nazionale di Geofisica e Vulcanologia, Centro Nazionale Terremoti, Via D. Creti, 12-40128 Bologna, Italy. Tel.: +39 051 4151433; fax: +39 051 4151498.
E-mail address: serpelloni@bo.ingv.it (E. Serpelloni).

0012-821X/$ – see front matter © 2010 Elsevier B.V. All rights reserved.
doi:10.1016/j.epsl.2010.08.005

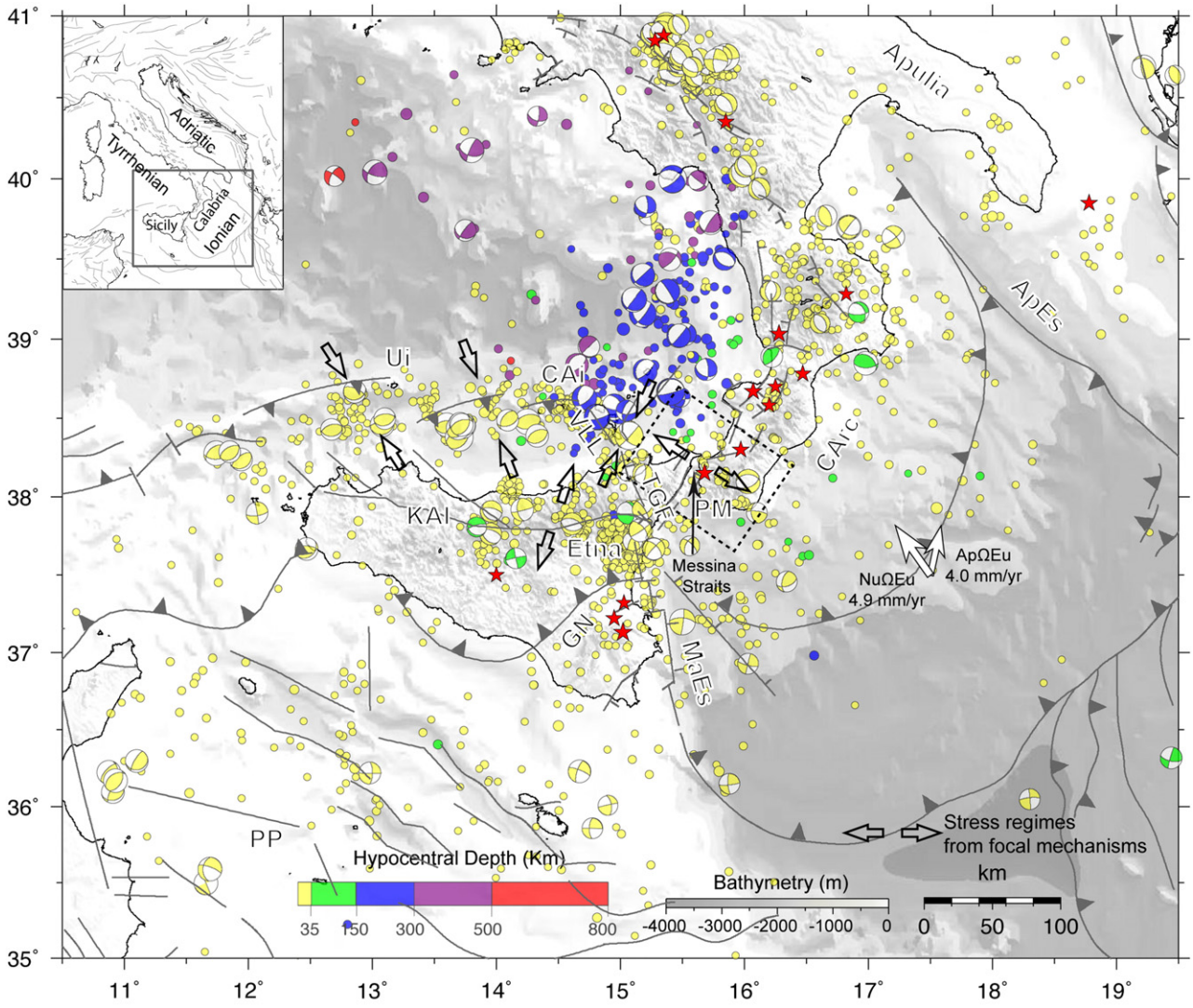

Fig. 1. Tectonic map of the Sicily and Calabria area. Grey lines show major fault systems (modified from the Geodynamic Map of the Mediterranean, compiled in the frame of the Commission for the Geological Map of the World, http://ccgm.free.fr). Earthquake focal mechanisms are taken from Harvard-CMT, INGV-RCMT and ETH-RMT catalogues. Instrumental seismicity is taken from Chiarabba et al. (2005), for the 1981–2002 interval, and from the INGV seismic bulletin (http://iside.rm.ingv.it) for the 2002–2009 time interval. Red stars show historical earthquakes with M ≥ 6.5 from the CPTI04 catalogue (available at http://emidius.mi.ingv.it/CPTI04). Stress regimes are taken from Neri et al. (2003). Ui = Ustica Island, CAi = Central Aeolian Islands, VLL: Vulcano–Lipari lineament; TGF: Tindari–Giardini Fault system; KAl: = Kumeta–Alcantara Fault system, PM = Peloritani–Messina area, CArc = Calabrian Arc, MaEs = Malta Escarpment, PP = Pelagian Plateau, ApEs = Apulian Escarpment, GN = Gela Nappe. White arrows show competing kinematic boundary conditions for the Ioian Sea, after (D'Agostino et al., 2008).

continuous GPS monitoring in Italy, mainly due to the development of the INGV-RING network (Avallone et al., 2010), and the availability of data from other non-permanent GPS networks in Sicily, re-surveyed in the framework of a recent national research program (Margheriti, 2008). In this work we analyze and interpret CGPS and EGPS data between 1994 and 2009.53, with the goal of understanding the current state of strain accumulation across the NE-Sicily and Messina Straits region, and we develop first-order models of the deformation using elastic dislocation methods.

Assuming that the observed velocity gradient across the Straits is due to slip on the Messina Fault and that all strain that accumulates interseismically is elastic, we first use GPS velocities to estimate the optimal geometry and slip-rates on a single planar dislocation locked above a certain depth. However, the velocity gradient across the Messina Straits is likely to be affected by the strain accumulation associated with other nearby active faults, for which our knowledge of the geometry and interseismic kinematics is limited or debated (Argnani and Bonazzi, 2005; Argnani et al., 2007; Billi et al., 2006; Ferranti et al., 2007; Monaco and Tortorici, 2000) making the determination of the Messina Fault parameters a challenging problem. In particular, the degree of coupling, and related elastic strain signal, of the subduction interface under the Calabrian arc are a matter of debate (D'Agostino et al., 2008; Devoti et al., 2008; Gutscher et al., 2006), but may directly impact inferences of fault behavior along the Messina.

The use of model optimization techniques in half-space dislocation models requires a certain number of GPS stations sampling details of the velocity gradient across the active fault under investigation. Consequently, this model approach cannot be used to study offshore faults or areas of poor geodetic coverage, such as along the active faults surrounding the Messina Straits. Using the geometric information for the Messina Fault derived from the local optimal dislocation model, and assuming simple a priori geometries of nearby faults, we use an elastic block-modeling approach (Meade and Hager, 2005), to complement the single-dislocation model. The block model accounts for both crustal block rotations and elastic strain accumulation across block-bounding faults, and provides first-order information about the impact of some of the unknown parameters of the active faults surrounding the Straits on the estimated Messina Fault slip-rate.

2. Geodynamics and tectonics setting

The Messina Straits is located in the Calabro–Peloritani Arc (Fig. 1), which lies along a segment of the Central Mediterranean plate boundary zone. Over the Neogene and Quaternary the evolution of this zone is interpreted in terms of slow relative Africa–Eurasia plate convergence and fast subduction and roll-back of the Ionian lithosphere beneath the Calabrian Arc, accompanied by fast back-arc extension in the Tyrrhenian Sea (Dewey et al., 1973; Gueguen et al., 1998; Faccenna et al., 2001; Rosenbaum et al., 2002; Malinverno and Ryan, 1986). Today, the Ionian slab is imaged by seismicity and seismic tomography (Chiarabba et al., 2005, Lucente et al., 2006, Piromallo and Morelli, 2003), which outline a continuous, SW–NE striking and NW-dipping, narrow and steep Benioff plane down to about 500 km (Mele, 1998).

Although the subduction of the Ionian lithosphere was characterized by vigorous trench retreat and back-arc extension at a rate of 50–70 mm/yr during the Neogene and Quaternary (Faccenna et al., 2001, Nicolosi et al., 2006), a large spectrum of geophysical and geological data document a major tectonic reorganization in the central Mediterranean around 0.8–0.5 Ma, when rapid trench migration and consequent Tyrrhenian back-arc extension essentially stopped (e.g., Faccenna et al., 2001; Goes et al., 2004). Proposed models for the present-day geodynamics of the Mediterranean include plate (edge) force interaction (e.g., Royden, 1993; Goes et al. 2004), subduction slab dynamics (Wortel and Spakman, 2000) and large-scale mantle flow (Doglioni, 1991). Recently, Faccenna and Becker (2010) showed that flow driven by smaller-scale density anomalies in the mantle can explain most of the observed microplate kinematics in the Mediterranean region.

The NE-Sicily and Calabria region is characterized by some of the highest rates of seismic moment release along the Nubia–Eurasia plate boundary (Serpelloni et al., 2007). Focal solutions of shallow earthquakes offshore northern Sicily outline a narrow E–W compressive belt, consistent also with geologic data (Pepe et al., 2005). East of the central Aeolian area extensional to strike–slip mechanisms occur along a NNW–SSE seismic lineament that runs from the central Aeolian Islands to Mount Etna and continues S-ward along the eastern Sicily escarpment (Musumeci et al., 2005; Pondrelli et al., 2004; Serpelloni et al., 2007). Shallow extensional seismicity also characterizes the Mt. Etna area, and a diffuse belt running ESE–WNW in northern Sicily (KAl in Fig. 1). The transition zone between these two domains approximately corresponds to the western lateral termination of the Ionian slab at depth of 100–200 km (Faccenna et al., 2004), and to the Vulcano–Tindari–Giardini Fault system at shallow depths (Argnani, 2009; Billi et al., 2006). The active tectonics inferred from focal mechanisms in Calabria is less well defined. However, extensional tectonics and regional uplift characterized the onshore Calabrian Arc during the last 0.8 Ma (Westaway, 1993), and strong historical normal-faulting earthquakes indicate that extension is the dominant style of faulting along its Tyrrhenian side.

GPS and seismological data (D'Agostino and Selvaggi, 2004; D'Agostino et al., 2008; Jenny et al., 2004; Hollenstein et al., 2003; Neri et al., 2003; Pondrelli et al., 2004; Serpelloni et al., 2005; Serpelloni et al., 2007) consistently locate the Messina Straits at the boundary between two different kinematic and tectonic domains, depicting NE-Sicily and Calabria as a key region for understanding of active geodynamic processes in the central Mediterranean. However, the general kinematic framework of the area continues to be debated.

Although most of GPS data show that the Tyrrhenian basin is not actively spreading, or at least at a fraction of the past rates, debate concerning the present-day Ionian–Calabria convergence rate and direction, and consequently the way this convergence is eventually accommodated along the plate boundary, arise from observations and interpretations of the kinematics of Sicily and Calabria with respect to the Eurasian and Nubian plates (D'Agostino and Selvaggi, 2004; D'Agostino et al., 2008; Devoti et al., 2008; Goes et al., 2004; Serpelloni et al., 2007).

The motion of Sicily with respect to Nubia has been interpreted either as evidence of an independent Sicilian microplate (Devoti et al., 2008; Serpelloni et al., 2007), or, together with the observed GPS velocities on Apulia, as the expression of a larger Ionian–Apulian plate, which would include the Hyblean plateau in SE Sicily, intermediate between Nubia and Adria (D'Agostino et al., 2008). The presence of an Ionian–Apulian plate, moving independently from Nubia, has been invoked to explain the observed kinematics along the Calabrian Arc, that Goes et al. (2004) interpreted in the framework of recent plate reorganization, causing the Calabrian and Ionian domains to be driven E-ward by the Hellenic slab pull.

3. GPS data and analysis

In 1987, the first GPS survey across the Messina Straits was performed with single frequency receivers (Anzidei et al., 1998), over the terrestrial network of Caputo et al. (1981). The same network, with some additional TyrGeoNet stations (Anzidei et al., 2001), has been re-occupied with dual frequency GPS receivers in 1994, partially in 2002 and 2004, and most recently in 2008 (Margheriti, 2008). In this work we present a new GPS velocity field obtained by combining data from the Messina Straits EGPS network and the INGV-RING CGPS network. We also analyze data from other GPS surveys performed over several non-permanent networks in the 1994–2007 time span, as already described in Serpelloni et al. (2005, 2007).

To compute GPS station velocities we follow a three-step approach, which includes: 1) the phase data processing, 2) the combination of solutions and 3) the time series analysis. In the first step, we use daily GPS phase observations to estimate station coordinates, hourly atmospheric zenith delay, orbital and Earth orientation parameters by means of the GAMIT 10.33 software (Herring et al., 2006), applying loose constraints to geodetic parameters and adopting standard procedures for the analysis of regional networks (e.g., Serpelloni et al., 2006). We apply the ocean-loading model FES2004 and use the IGS (International GNSS Service) absolute antenna phase center models for both satellites and ground-based antennas.

In addition to GPS data from stations around the Messina Straits, we analyze data from more than 700 CGPS stations operating in the Euro–Mediterranean and African regions from 1 January 1994 to 20 July 2009, which are divided into about 30 sub-networks. The CGPS and EGPS sub-networks are processed independently, following the same procedures. A number of high quality CGPS sites are included in all solutions, and are used to tie together the daily loosely constrained solutions in the second step of our analysis. The common CGPS sites are chosen among the stations showing the highest data continuity through time, in order to ensure that a minimum number (always >3) of sites are in common to all sub-network solutions.

In the second step we use the ST_FILTER program of the QOCA software (Dong et al., 2002) to combine all the daily loosely constrained solutions, for both CGPS and EGPS sub-networks, with the global and regional solutions made available by SOPAC (http://sopac.ucsd.edu), and simultaneously realize a global reference frame by applying generalized constraints (Dong et al., 1998). Specifically, we define the reference frame by minimizing the horizontal velocities of the 132 IGS-core stations (http://igscb.jpl.nasa.gov), while estimating a seven-parameter transformation with respect to the IGS05 realization of the ITRF2005 NNR frame (Altamimi et al., 2007). In order to account for offsets observed in the time series of some IGS-core sites (due to earthquakes or changes in the receiver/antenna configuration that could contaminate the combined solution), we estimate the offset parameters of the IGS-core sites in a preliminary ST_FILTER run of the IGS daily solutions only, and then use the estimated values to correct the reference frame jumps in the final

combination and reference frame realization. Reference frame stability through time is ensured by the presence of at least 40 IGS-core sites that are continuously present in SOPAC solutions from 1994 to present-days.

In the third step we analyze the position time series in order to estimate absolute IGS05 velocities and uncertainties for both CGPS and EGPS stations. In particular, for the CGPS stations we estimate a constant velocity term together with annual and semi-annual seasonal terms and, if present, offsets at specific epochs. For the EGPS stations we only estimate the constant velocity term. Detrended position time series of the EGPS stations used in this work are shown in Fig. S1 of the Supplementary material. Given the large uncertainties associated with vertical EGPS positions and rate estimates, and the fact that most of CGPS stations in NE-Sicily and Calabria have short (<3.5 years) time spans, in this work we use only the horizontal GPS velocities.

Realistic velocity uncertainties are evaluated adopting a white-plus-colored noise model following the maximum likelihood estimation approach implemented in the CATS software (Williams et al., 2004), and the procedures described in (Williams, 2003). In particular, for CGPS stations we adopt a white + flicker noise model (see Table S1), whereas for EGPS stations we adopt an error model that combines white + random walk noise using a value of 1 mm/yr$^{0.5}$ for the random walk component (Hammond and Thatcher, 2004; Langbein and Johnson, 1997; Dixon et al., 2000, Beavan et al., 2002). We use velocities and uncertainties of CGPS stations located on tectonically stable domains of the Eurasian and Nubian plates in order to estimate their Euler rotation vectors with respect to the IGS05 frame. The Euler pole parameters of major plates and of the Apulian microplate are given in Table S2 of the Supplementary material. The observed and residual velocities of CGPS sites used to define the three reference frames are given in Table S3 of the Supplementary material, and Fig. S3 shows the location of the estimated Nubia–Eurasia pole with respect to previously published values.

Station positions, horizontal linear velocities and uncertainties in the IGS05 and Eurasian fixed reference frames, are listed in Table S4 and Table S5 of the Supplementary material. We only incorporate data from CGPS stations with an observation period longer than 2.5 years, as shorter intervals may result in biased estimates of linear velocities (Blewitt and Lavallee, 2002). Fig. 2 displays horizontal velocities with respect to the Eurasian fixed frame for GPS stations in the Sicily and Calabria area.

4. Velocity and strain rate fields

Fig. 2 illustrates some first-order features of the regional GPS velocity field, showing a smooth transition between two clearly distinguishable velocity domains in Sicily and Calabria, as already highlighted by D'Agostino and Selvaggi (2004), Serpelloni et al. (2007) and D'Agostino et al. (2008). GPS velocities in the Sicily

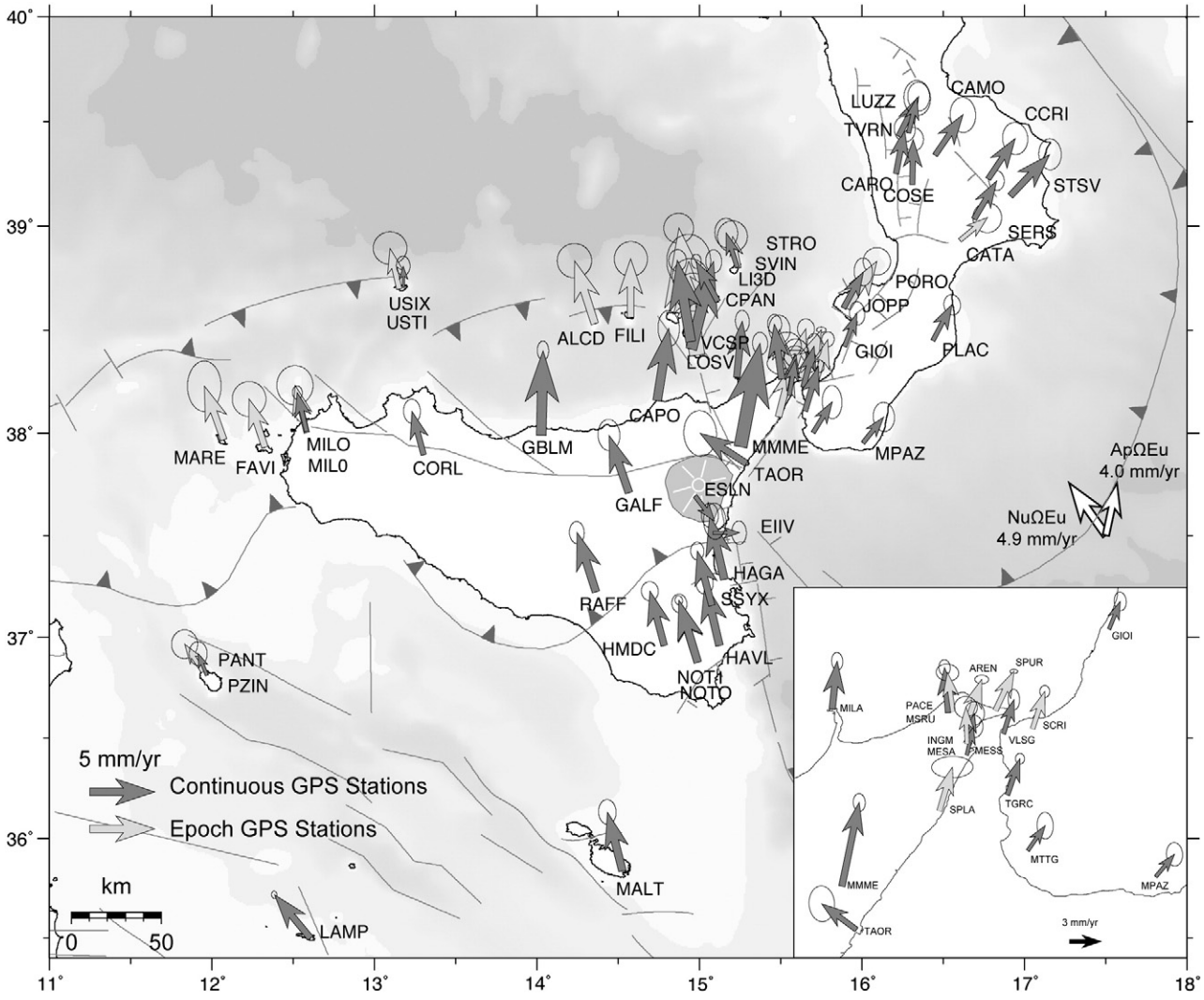

Fig. 2. GPS velocity field with respect to the fixed Eurasian frame defined in this work (Table S2). Error ellipses are at 95% confidence level.

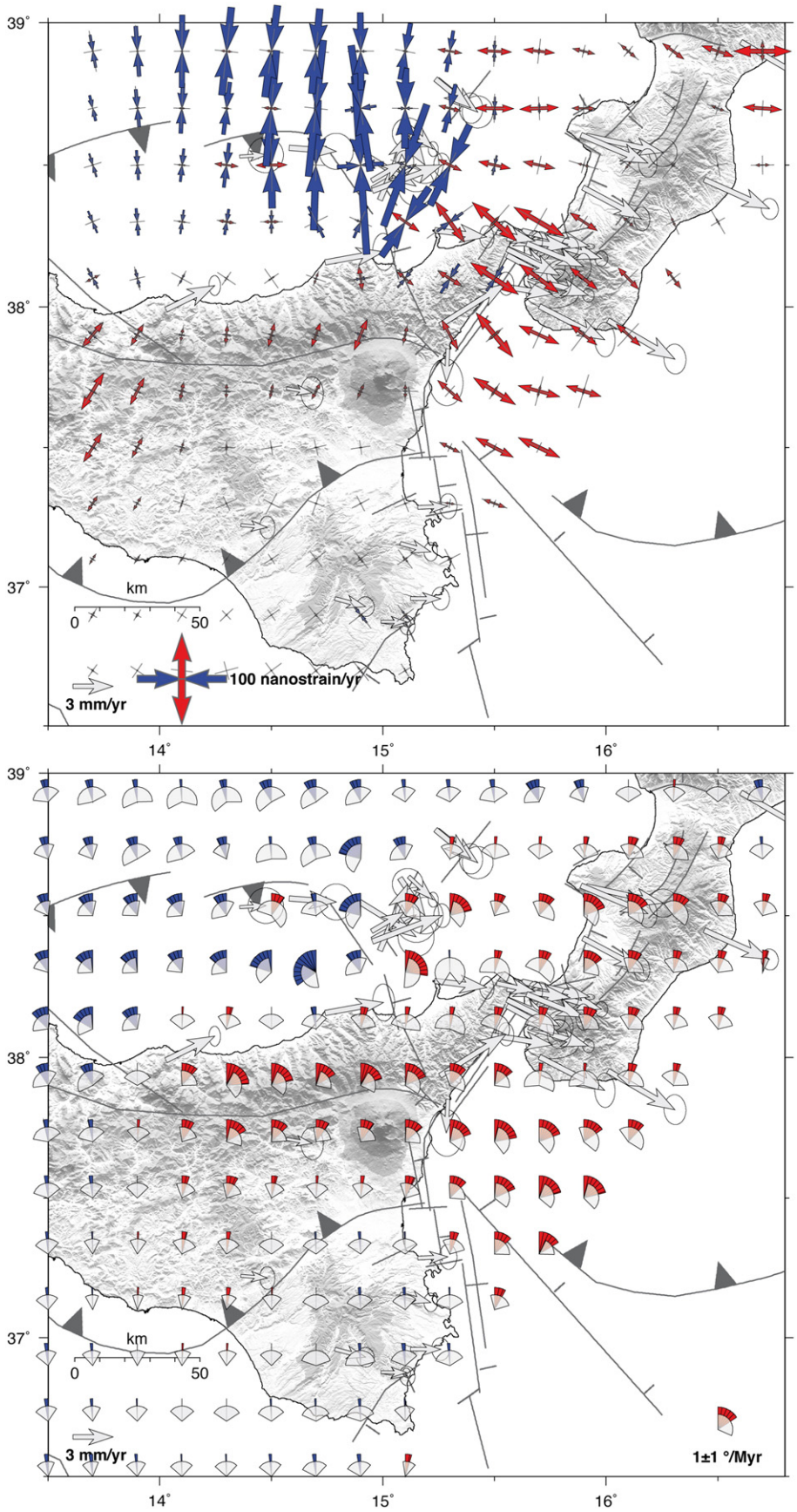

Fig. 3. Geodetic strain rate field computed over a regular 0.2°×0.2° grid. [Top] Red and blue arrows show extensional and compressional strain rates, respectively. Grey crosses display 1σ uncertainties. [Bottom] Rotation rates and 1σ uncertainties (grey wedges). Red wedges show clockwise rotations, whereas blue wedges show counter-clockwise rotations. Grey arrows in both panels show GPS velocities with respect to the Nubian fixed frame defined in this work (Table S2).

domain are in general agreement with the NW-ward motion of the Nubian plate with respect to Eurasia, although, residual motion of stations in Sicily and the Pelagian area (i.e., LAMP and MALT) with respect to Nubia (Fig. S4) suggest that this region is moving independently from both Nubia and Eurasia. A few stations in eastern Sicily (i.e., EIIV and ESLN) show E-ward oriented velocities that may be related to local deformation of Etna volcano (Lundgren et al., 2004; Bonforte and Puglisi, 2006). As these velocities are not representative of the regional microplate kinematics, they have been excluded from the analysis of the velocity gradient field. In northern Sicily, more rapid northward motion of some stations is observed north of the Kumeta–Alcantara lineament. NE-Sicily GPS velocities rotate clockwise, moving to a NE-ward direction that is about normal to the predicted Nubian plate motion. At a more local scale, our new GPS velocity solution outlines a fan-like pattern of the velocity vectors across the Messina Straits, where velocities undergo a clockwise rotation of about 30°, from north to south.

In order to better characterize the regional and, where allowed by the GPS network geometry, local features of the contemporary crustal deformation field, we use the horizontal velocities of stations located in Eastern Sicily and Western Calabria to invert for the velocity gradient tensor field. We use the approach described in Shen et al. (1996) that provides an interpolated velocity gradient field starting from a discrete set of GPS stations accounting for velocity uncertainties, network geometry and inter-station distances. Strain and rotation rates are estimated from the velocity data and uncertainties through weighted least squares on a regular 0.2°×0.2° grid, extending between longitude 13.5°E–16.8°E and latitude 36.5°N–39°N. The contribution of each station in the least squares inversion is scaled by a Gaussian function $exp(-\Delta R^2/D^2)$, where ΔR is the distance between a geodetic station and the grid point being evaluated and D is a smoothing distance that is optimally determined, within a priori defined bounds, through balancing the trade-off between the formal strain rate uncertainty estimate and the total weight assigned to the data (Shen et al., 2007). The re-weighting determines the degree of smoothing around a given spot and the uncertainties of the strain estimates, while the optimal D value can be considered as an indicator of how local or regional the strain rate tensor inverted at each grid point is (i.e., stations within the scaling distance D contribute more than 68% to the least squares solution; Shen et al., 2007).

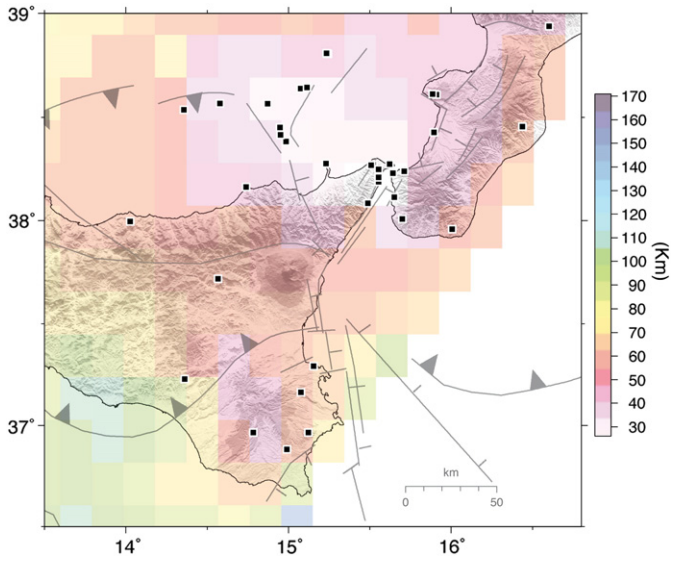

Fig. 4. Spatial variation of the distance decay value (D, in km), used to rescale the velocity data in the least squares inversion of the strain rate field of Fig. 3. The D value may be considered as an indicator of how local or regional the strain rate tensor inverted at each grid point is. We obtain values ranging between 20 and 100 km, with a typical value of ~60 km. The image is obtained by gridding of discrete D values over the 0.2°×0.2° regular grid used to compute the strain rate field.

Fig. 3 shows the horizontal principal strain rates and rotation rates, with 1σ uncertainties, together with GPS velocities given with respect to the Nubian plate. Fig. 4 shows an image of the distance decay value (D), for which we obtain values ranging between 20 and 100 km, and a typical value of ~60 km. It is worth noting that strain rates across the Straits are computed with D values of about 20 km, making our estimates a local measurement of the deformation across it. Fig. S5 in the Supplementary material displays the maximum shear and dilatation rates.

Two stations in NE-Sicily, MMME and TAOR that are close each other, display some inconsistency in their velocities. Although their position time series do not show any significant problem in the data, the observed difference may be due to suspected monument instability at both stations (INGV-Catania, personal communication). Anyway, we found that the strain-rate tensors inverted across the Straits are not significantly influenced by these two stations, indicating that the data available across the Straits are strong enough to allow a local estimate of the current strain rate field.

Higher deformation rates occur in the Peloritani–Messina and Central Aeolian area (Fig. 3 and Fig. S5). The SE Tyrrhenian is characterized by fast (up to ~200 nanostrains/yr) shortening, which rotates from N–S to SW–NE direction across the Salina–Lipari–Vulcano tectonic lineament. Fast shortening rates in the Central Aeolian Islands have been associated with the interplay between convergence of the Sicily and Tyrrhenian domains and volcano-tectonic deformation (Mattia et al., 2008; Serpelloni et al., 2007), whereas the NE–SW oriented shortening has been related to an actively deforming submarine anticline between Cape Milazzo and the Aeolian Is. (Argnani et al., 2007). The inferred continuation of the contraction to the north of the islands is from the high D value and smoothing (Fig. 4), but is not fully constrained by data since no GPS sites (i.e., islands) are available for some distance to the N. Rapid NW–SE oriented extensional deformation rates (up to ~65 nanostrains/yr) characterize the Peloritani and Messina Straits, about normal to its coastlines. The almost purely extensional deformation regime observed across the Messina–Peloritani region is consistent with the dominant extensional faulting here. Significant extensional deformation, but at lower rates, is also inferred along the Tyrrhenian side of the Calabrian Arc and, on-land Sicily, along a EW oriented belt that corresponds to the distributed extensional tectonic belt (Fig. 1) along the Kumeta–Alcantara lineament. On the contrary, no significant strain is observed across the Apennines thrust belt (i.e., the Gela Nappe in Fig. 1).

With regards to the antisymmetric part of the velocity gradient field, statistically significant rotation rates (Fig. 3) are present across the Kumeta–Alcantara Fault zone, in northern Sicily, and across the Vulcano–Tindari–Giardini Fault lineament, in the southern Tyrrhenian Sea. The clockwise rotations in northern Sicily agree with those estimated in southern Calabria, where paleomagnetic data also demonstrate clockwise rotations in the uppermost Lower Pleistocene–Middle Pleistocene terrains (Cifelli et al., 2008). Importantly, in the Peloritani Mts. and across the Messina Straits rotations are close to zero. The geodetic rotations in the southern Tyrrhenian Sea, and in particular the change from fast counter-clockwise to fast clockwise rotation rates across the Vulcano–Tindari–Giardini lineament, are more difficult to interpret. This complex fault system has been interpreted as a Subduction–Transform–Edge Propagator (STEP) Fault (e.g., Argnani, 2009; Carminati et al., 1998). Numerical models for STEP faults (Govers and Wortel, 2005) show that significant rotations are expected along such faults, although additional complexities may be attributed to the upper plate response to deep-seated processes. The complex pattern of geodetic rotations across the central Aeolian Is. suggests the presence of an important kinematic discontinuity, although its investigation is beyond the scope of this work.

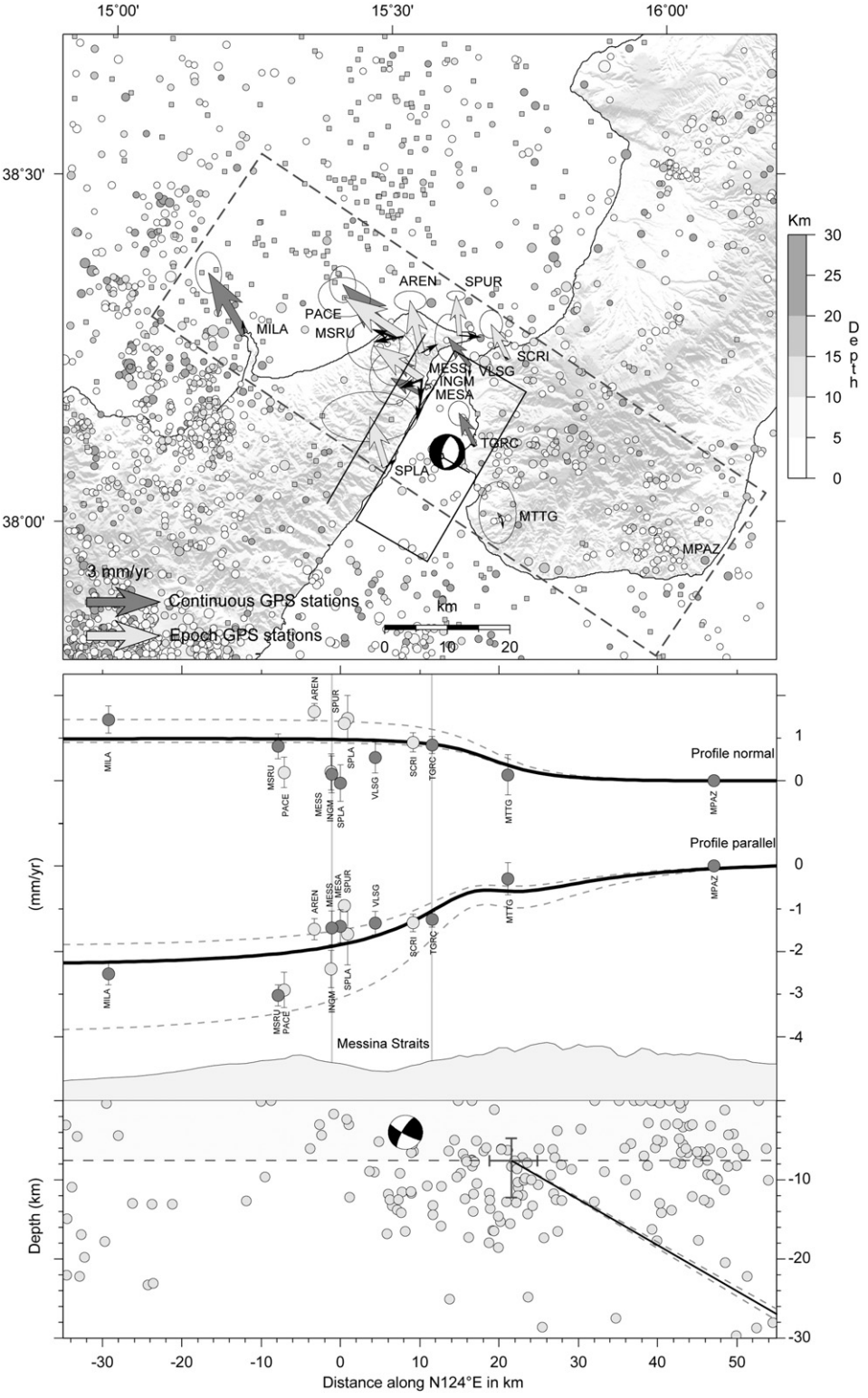

Fig. 5. [Top]. Horizontal observed velocities with respect to station MPAZ and model residual velocities (black arrows). Seismicity from the CSI-1.1 earthquake catalogue (Chiarabba et al., 2005) is also reported (circles in grey colors show crustal seismicity, within 0–30 km depth, whereas grey squares show deeper seismicity). The beach ball shows the Messina 1908 earthquake focal mechanisms from (Boschi et al., 1989). The black box shows the Messina Fault source as described in the DISS database (http://diss.rm.ingv.it/diss/). [Bottom] N124°E (i.e., parallel to the direction of maximum elongation from Fig. 3) cross section showing the horizontal velocity gradients (both the profile-normal, dip–slip, and profile-parallel, strike–slip, components) given with respect to station MPAZ, from optimally inverted fault parameters and slip-rates (grey line). The light grey dotted lines display fault slip-rate 68% confidence error bounds from the bootstrap analysis. Dark grey and light grey, with 1σ uncertainties error bars, show EGPS and CGPS stations, respectively. The topographic profile is also shown, together with a cross section of crustal seismicity (including the 1908 earthquake focal mechanism from Boschi et al., 1989) and the modeled geometry and 68% uncertainties from the bootstrap percentile method (see Table 1).

5. Messina Fault dislocation model

The strain rate field of Fig. 3 shows that the contemporary tectonic regime in the Peloritani–Messina region is dominated by active NW–SE extension. The way the observed velocity gradient (see Fig. 5) is presently accommodated by faulting and the number of faults that may take up this deformation is presently unclear, but very important for the evaluation of the associated seismic hazard. We explore this question by first examining very simple dislocation models that try to explain the local Messina Straits velocities in the context of elastic deformation about a single locked normal fault.

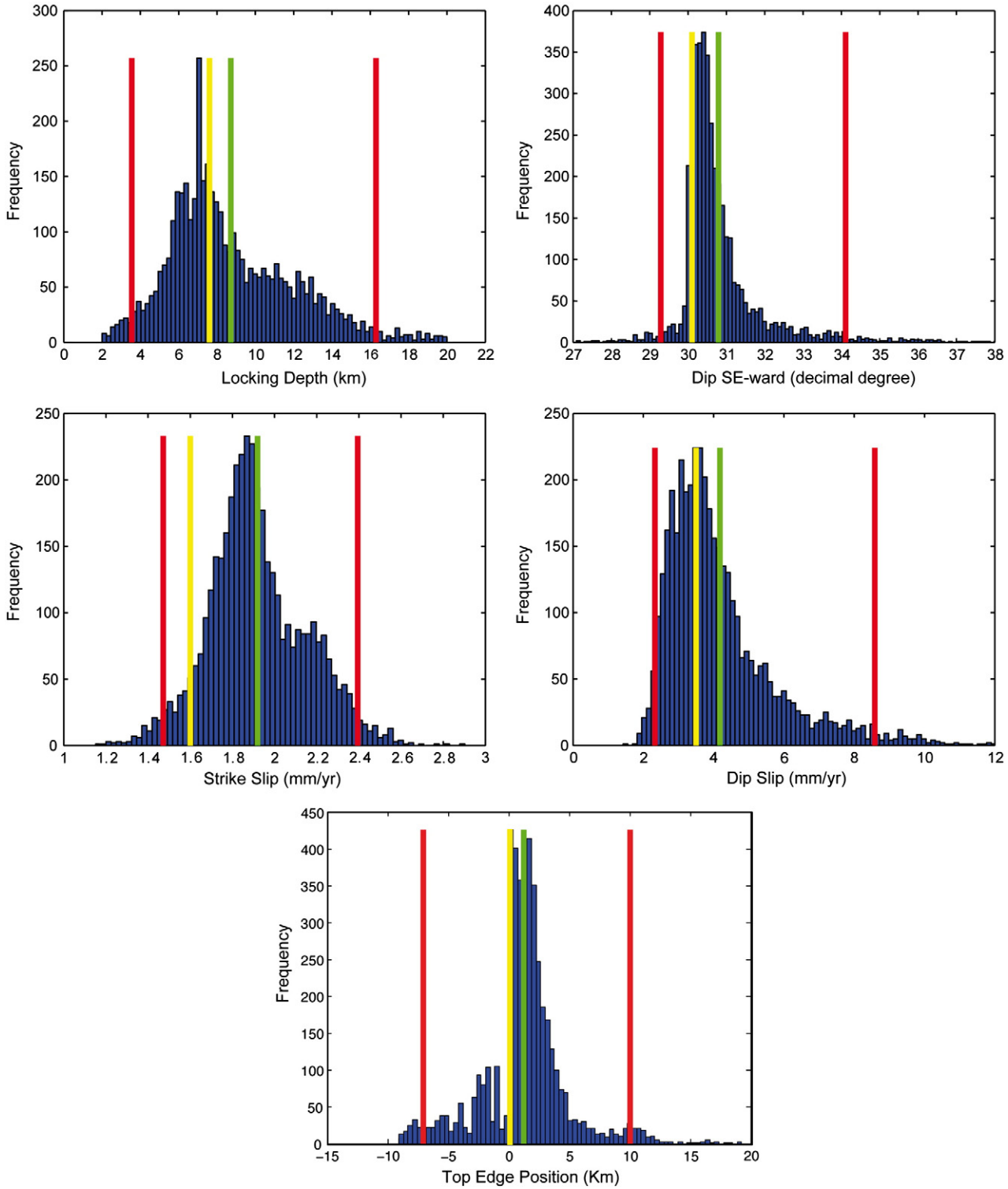

Fig. 6. Frequency histograms of modeled fault parameters from 5000 bootstrap re-samples of the original data. Red lines mark lower and upper bounds values of 95% confidence level, evaluated adopting the bootstrap percentile method (Arnadottir and Segall, 1994). Green and yellow lines mark mean and optimal values of each parameter, respectively. The values in the top-edge position panel refer to distances in km from its optimally determined position.

The horizontal GPS velocities allow us to develop first-order models of the deformation using elastic dislocation theory, assuming that the observed velocity gradient across the Messina Straits, showing that ~3 mm/yr of NW–SE extension are accommodated across it, results from the elastic deformation of the brittle crust in response to plate displacement away from the fault zone and ductile shear at depth. The model explicitly assumes aseismic creep beneath a given depth (i.e., the fault locking depth) at rates that should be comparable with the long-term tectonic loading (Savage and Burford, 1970).

We use rectangular (Okada, 1985), uniform-slip dislocations embedded in an elastic, homogeneous and isotropic half-space and a constrained, non-linear optimization algorithm (Burgmann et al., 1997), to solve for the best fit rectangular dislocation geometry (parameterized by length, depth, width, dip, strike, and fault edge location) and fault slip-rates (both dip–slip and strike–slip components). Our inversions aim to find model parameters that minimize the weighted residual sum of squares $WRSS = (d_{obs} - d_{mod})^T \times cov^{-1} \times (d_{obs} - d_{mod})$, where d_{obs} and d_{mod} are the observed and modeled motions, respectively and cov is the data covariance matrix. We use 14 GPS stations (Fig. 5) across the Straits and assume a quasi-2D model geometry (i.e., we constrain the fault length and width to very large values). On the basis of the computed strain rate field (Fig. 3) we constrain the fault strike to be perpendicular to the maximum extensional strain (i.e., oriented about N34°E) and explore all other parameters.

To estimate the individual confidence intervals associated with the inverted model parameters, we employ a bootstrap method (Arnadottir and Segall, 1994), which establishes confidence intervals by randomly re-sampling from the data, with replacement, and running the parameter optimization n-times. Fig. 6 displays histograms of the inverted model parameters obtained from 5000 random bootstrap re-samples, together with the corresponding mean values and uncertainties. The optimal ($WRSS/N = 3.7$) model fault geometry and slip-rates are reported in Table 1 together with 68% and 95% confidence intervals estimated using the bootstrap percentile method. We find that to first-order, the observed velocity gradient across the Straits can be explained by a single $30.1^{-0.7}_{+1.1}$° SE-dipping normal fault, locked at $7.6^{-2.9}_{+4.6}$ km depth, and a dip–slip-rate of $-3.5^{-1.3}_{+2.0}$ mm/yr and a right-lateral slip-rate of $1.6^{-0.2}_{+0.3}$ mm/yr. Fig. 5 shows observed and residual velocities relative to station MPAZ, and the velocity profiles (i.e., both profile-normal and profile-parallel components) across the Messina Straits, including the modeled velocity gradients from the inverted fault parameters. While observed CGPS velocities are well matched by the model velocity gradient, velocities of EGPS stations on the Sicilian side of the Messina network display larger residuals. MSRU and PACE, in particular, for which horizontal velocities are rather well constrained (see Table S4, Table S5 and Fig. S1), display the largest residuals on a strike-perpendicular direction.

6. Regional elastic block model

In the previous section we modeled the velocity gradient across the Messina Straits assuming it is due to a single normal fault accumulating elastic strain. However, the area is surrounded by other active fault zones that are likely to be interseismically accumulating elastic deformation, among which the Tindari–Giardini Fault system to the W, the Calabrian normal fault system to the NE and the Calabria subduction interface to the SE, are the most important ones (Figs. 1 and 7). Unfortunately, our knowledge of the geometry and kinematics of these faults is quite incomplete (Argnani et al., 2007; Billi et al., 2006; D'Agostino and Selvaggi, 2004; Ferranti et al., 2007; Gutscher et al., 2006). As they are located offshore, and/or poorly covered by GPS networks, it is not possible to develop any optimal geometry and kinematic inversions outside the Messina Straits. However, we find that it is important to evaluate the impact of elastic strain fields from these faults on the inferred slip-rates of the Messina Fault, especially from the far-reaching strain of the potentially seismogenic Calabrian subduction thrust.

To test if the velocity gradient across the Messina Straits may be significantly modified by the elastic strain contribution from these three fault systems we use an elastic block-modeling approach that accounts for both crustal block rotations and strain accumulation at block-bounding faults (Meade and Hager, 2005). The spatial extent of surface interseismic strain of a block-bounding fault depends on its degree of coupling, which is parameterized by changing the width of its locked portion. Increasing the locking width increases the magnitude and reach of elastic deformation associated with the fault, which changes the optimal block rotation parameters and fault slip-rates in the optimal model. For each investigated fault system, we run suites of model inversions using different values of the locking depth, and evaluate the trade-off curves between the model reduced χ^2 and the Messina Fault slip-rate (the dip–slip component) as a function of increasing values of assumed locking depth.

Importantly, the convergence rates across the Ionian–Calabrian subduction interface differ by a factor of two depending on which plate the Ionian oceanic lithosphere belongs to. The SE-ward displacements of the Calabrian stations with respect to the Ionian block occur at rates of ~5 mm/yr and ~2.5 mm/yr with respect to Nubia or to the Ionian–Apulian plate, respectively (see Fig. 7). Therefore, it is of fundamental importance for the evaluation of the seismic potential of the Calabrian region to understand how this convergence is eventually accommodated along the subduction interface, and if its deformation signal may be overprinted on the measured velocity gradients across the Messina Straits. An Ionian-fixed velocity field is the appropriate reference frame realization for our objective, allowing us to implement a relatively simple block geometry while accounting for the two end-member kinematic boundary conditions along the Ionian–Calabria plate contact. This is realized by implementing two different experiments (see Fig. 7), the first one considering the Ionian block as part of Nubia (i.e., using Nubia-fixed velocities), and the second one considering the Ionian block as part of the Apulian microplate (i.e., using Apulia-fixed velocities).

We use seismicity, fault maps (see Fig. 1), fault databases (Basili et al., 2008, Meletti et al., 2008) and other indicators of active deformation along the central Mediterranean Africa–Eurasia plate boundary (Serpelloni et al., 2007) to define the model geometry (i.e., numbers of blocks, strike, dip and locking-depths of block-bounding faults). We consider a relatively simple block configuration, where Sicily, Calabria, the Tyrrhenian lithosphere and the southern Adriatic

Table 1
The upper row shows the values of optimally inverted model parameters estimated with the non-linear inversion algorithm. The bottom rows show the mean values, obtained by running inversion with 5000 bootstrap re-samples of the original data, with 68% and 95% confidence level intervals, estimated using the bootstrap percentile method (Arnadottir and Segall, 1994). The fault top-edge position [a] is given as the distance (in km) of the mid-point from a line parallel to the modeled fault plane and crossing the Messina (MESA) GPS station. The bootstrap confidence bounds are given in terms of distance (in km) from the optimally determined fault plane top-edge.

	Locking depth (km)	Dip SE-ward (decimal degrees)	Strike–slip (mm/yr)	Dip–slip (mm/yr)	Top-edge position (km)
Optimal model	7.6	30.1	1.6	3.5	21.68[a]
Bootstrap (68% c.l.)	$8.8^{-2.9}_{+4.6}$	$30.08^{-0.7}_{+1.1}$	$1.9^{-0.2}_{+0.3}$	$4.1^{-1.3}_{+2.0}$	$1.24^{-2.8}_{+3.2}$
Bootstrap (95% c.l.)	$8.8^{-5.1}_{+7.5}$	$30.08^{-1.5}_{+3.3}$	$1.9^{-0.4}_{+0.5}$	$4.1^{-1.8}_{+4.4}$	$1.24^{-8.3}_{+8.7}$

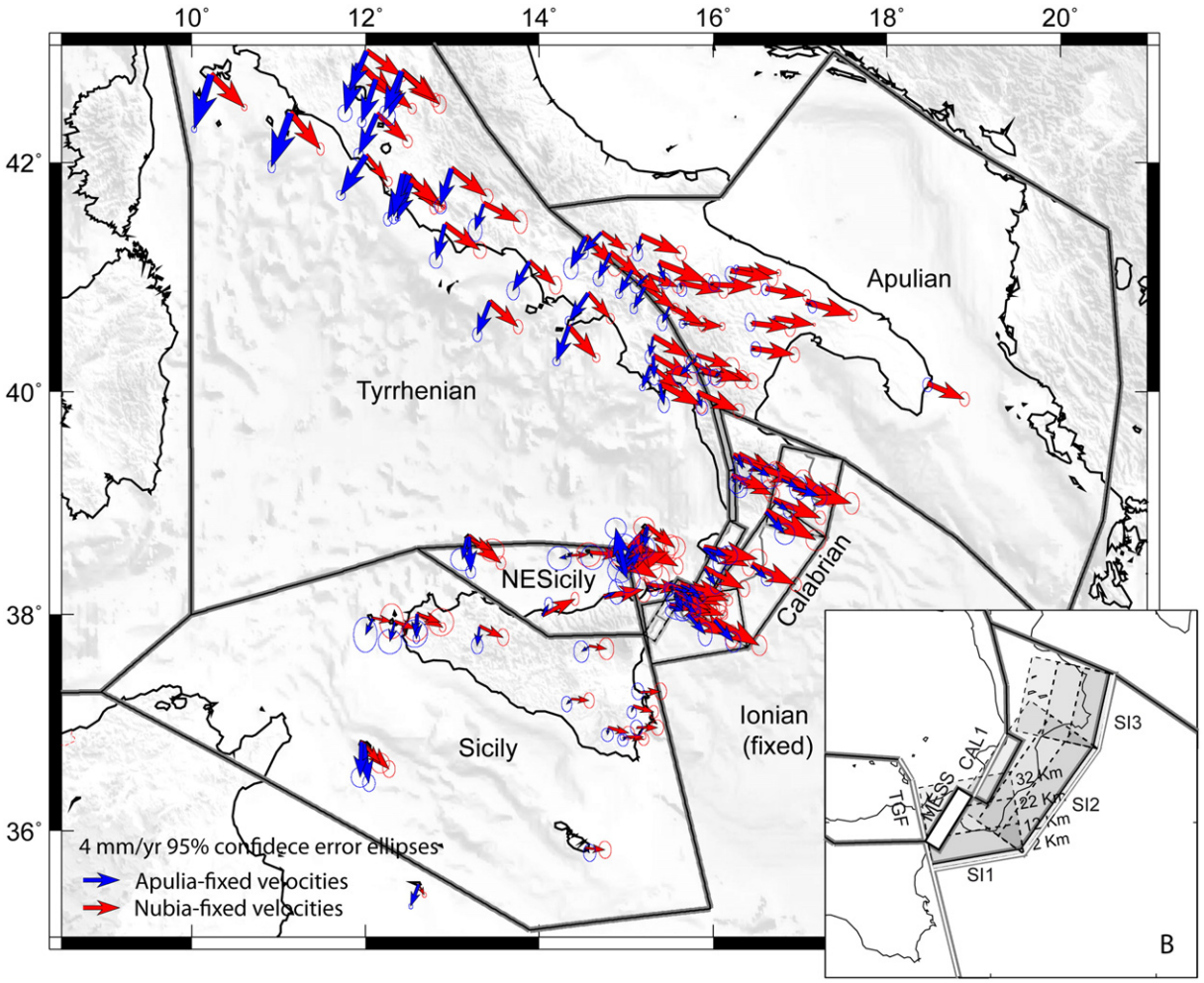

Fig. 7. Block model geometry and horizontal GPS velocities (with 95% confidence ellipses) rotated into the Apulia-fixed (blue arrows) and Nubia-fixed (red arrows) reference frames defined in this work (see Table S2), respectively. [B] Fault systems investigated in this work, keeping fixed the geometry of the Messina Fault (MESS) at the values obtained from the local dislocation model (Table 1). For the western Calabrian normal Fault system (CAL1) and the Tindari–Giardini Fault system (TGF) the locking depth varies from 0 to 20 km, whereas for the Calabrian subduction interface (SI1, SI2, and SI3) the locking depth varies from 0 to 40 km.

region (i.e., Apulia) behave as independent blocks with respect to the Ionian lithosphere, used as the reference micro plate (Fig. 7). A more detailed analysis of the microplate settings and kinematics of the study area is beyond the scope of this work, and we adopt the same block geometry (i.e., the same number of inverted parameters) with both experiments. In order to represent the Ionian–Apulian microplate, as proposed by D'Agostino et al. (2008), when running the models with Apulia-fixed velocities we constrain the southern Adriatic block to not rotate with respect to the Ionian block.

We use vertical planar dislocations and a regional locking depth of 10 km, consistent with average depths to the base of crustal seismicity (Chiarabba et al., 2005) and values reported in the DISS database (http://diss.rm.ingv.it/diss/), for all block-bounding faults, except for the Messina and Calabrian normal faults and the NW-ward dipping subduction interface (Fig. 7). For the Messina Straits Fault we use the geometry (i.e., strike, dip and locking depth) derived from our local inversion (Table 1). For the western Calabria normal fault system we adopt the geometry reported in the DISS database. The subduction interface is parameterized by three 20° NW-dipping planes, whose first-order representation has been obtained from the analysis of cross sections of instrumental seismicity across the Calabrian Arc, and geological and geophysical data (Cernobori et al., 1996) together with general constraints from slab geometry. Importantly, as we effectively model the shear zone down-dip of a zone assumed to be fully locked, we cannot address to what degree shallow, distributed or localized accretionary-wedge deformation occurs interseismically.

Fig. 8 shows that changing the degree of coupling of the Tindari–Giardini Fault system (A and A′) does not significantly affect the slip-rates of the Messina Fault, and the impact on the reduced model χ^2 is minimal for both kinematic boundary conditions. Changing the degree of coupling of the western Calabria normal fault system (B and B′ in Fig. 8) also has little impact on the model χ^2; however, slip-rates of the Messina Fault increase by about 1 mm/yr for both kinematic boundary conditions, as the imposed locking width changes from 0 to 20 km on the western Calabria normal faults. On the contrary, we find that changing the locking width of the subduction interface (C and C′ in Fig. 8) has a large impact on the model χ^2 statistics and on the Messina Fault slip-rates for both kinematic boundary conditions.

Inferred dip–slip-rates on the Messina Fault are strongly impacted by the assumed locking width of the Calabrian subduction thrust. Assuming that the Ionian lithosphere is moving with the Nubian plate, the optimal Messina dip–slip rate varies between ~0 and −5 mm/yr as the subduction interface locking width is changed (Fig. 8). The slip-rate corresponding to the model χ^2 minima (reached for a 22 km locking depth, or 64 km down-dip width) is ~−1 mm/yr, whereas a subduction interface locked to only 16 km results in a −5 mm/yr value. Assuming that the Ionian lithosphere is moving together with

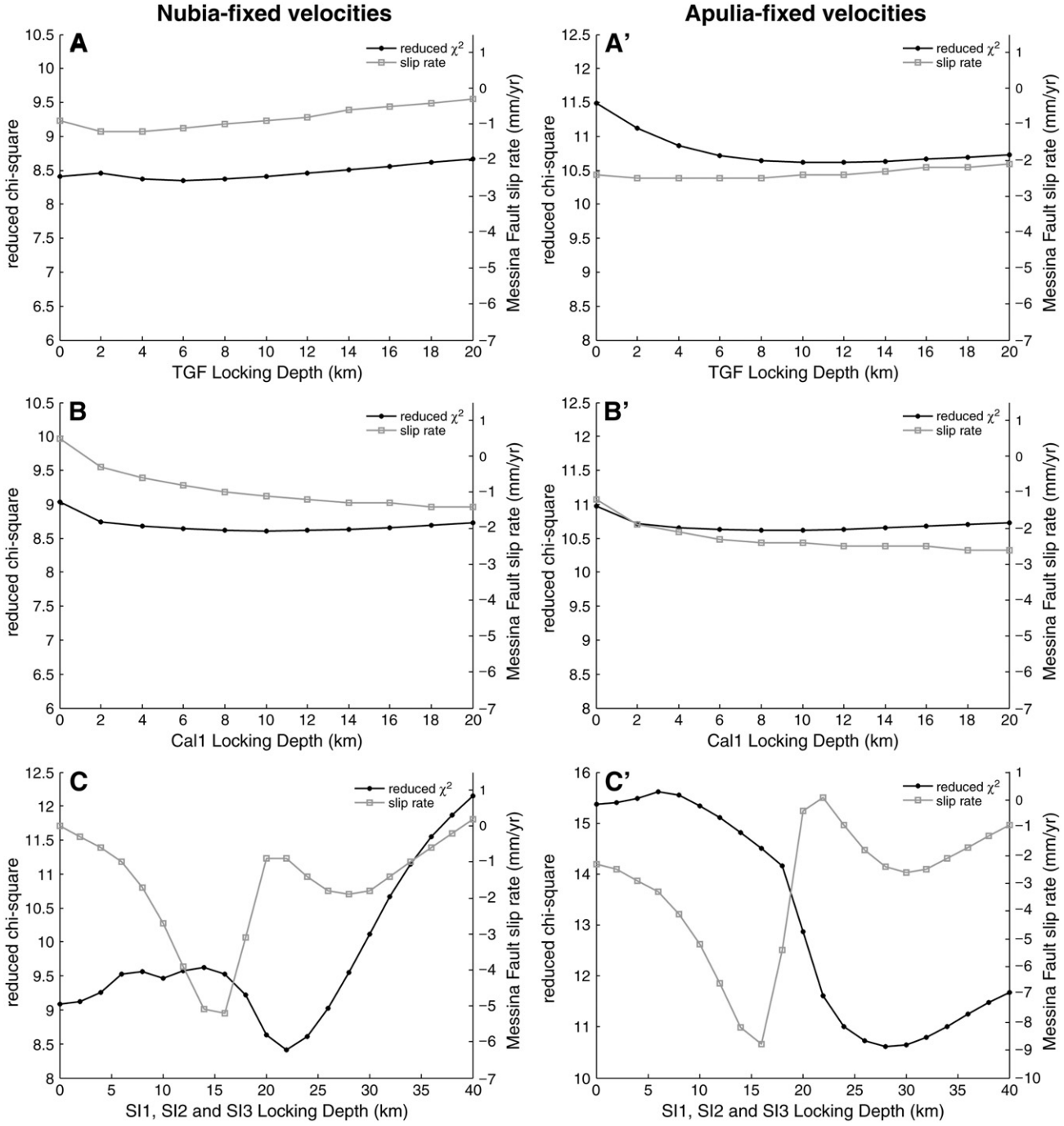

Fig. 8. Plots of the variation in the reduced chi-square values (black lines) and Messina Fault dip slip-rates (grey lines; negative values correspond to extension) obtained from the block-modeling by varying the locking-depths of the Tindari–Giardini Fault system (TGF in Fig. 7; A and A′ in this figure) from 0 to 20 km, the western Calabria normal fault system (Cal1 in Fig. 7; B and B′ in this figure) from 0 to 20 km, and the Calabrian subduction interface (SI1, SI2 and SI3 in Fig. 7; C and C′ in this figure) from 0 to 40 km. [Left] Results obtained using Nubia-fixed velocities (see Fig. 7), that is, assuming that the Ionian block moves like the Nubian plate toward Calabria. [Right] Results obtained using Apulia-fixed velocities (see Fig. 7), that is, assuming that the Ionian block moves like the Apulian microplate toward Calabria. By having different relative velocities across the subduction thrust, the only parameters that change in the two experiments are the rotational parameters and the slip-rates of the blocks that share a boundary with the Ionian block, and this does impact the Messina Fault slip-rate inverted from the GPS data under the two respective kinematic frameworks.

the Apulian microplate, the Messina Fault dip–slip-rate varies between 0 and −9 mm/yr. In this case, the χ^2 minima is reached for a locking depth of 28 km of the subduction interface (i.e., 81 km down-dip width), with a dip–slip-rate of the Messina Fault of −2.5 mm/yr. It is worth noting that in both cases, the block-modeling inferred Messina Fault slip-rate is smaller than the slip-rate obtained from optimal inversion of the local horizontal velocities in the previous section. Fig. S6 of the Supplementary material shows residual velocities and block-bounding fault slip-rates obtained adopting the locking depth value of the subduction interface corresponding to the χ^2 minima in Fig. 8, and the Euler pole parameters for the two configurations are reported in Table S6 of the Supplementary material.

Given our lack of knowledge about the shallow subduction interface geometry and coupling, we believe that additional geophysical and geological data are needed to allow for developing and testing of different and more detailed dislocation models of the subduction interface. Moreover, the availability of well constrained vertical motion rates in Calabria will certainly help in evaluating different

competing models, since the long-wavelength vertical subduction signal should be significant, in case of substantial plate interface coupling (e.g., Matsu'ura and Sato, 1989).

7. Discussion and conclusions

We use data from permanent GPS networks and a smaller aperture non-permanent GPS network to study the kinematics and active strain accumulation in the area affected by the destructive 1908 Messina–Reggio Calabria, $M_w = 7.1$, earthquake. GPS velocities define a well constrained kinematic pattern (Fig. 2), where, in a fixed Eurasian reference frame, stations located in Sicily move NW-ward at an average rate of ~4.5 mm/yr, whereas stations in Calabria move NE-ward at average rates of ~3.2 mm/yr. Faster N-ward motion rates are observed in NE-Sicily, whereas across the Peloritani Mountains and the Messina Straits velocities rotate from N-ward to NE-ward, and this trend continues along Calabria. GPS velocities with respect to a fixed Nubian reference frame (Fig. S4) show that, in Sicily, stations located south of the Kumeta–Alcantara Fault zone move toward the Ionian Sea at ~2.0 mm/yr, while stations north of it move ENE-ward at higher rates (~4 mm/yr). GPS stations in Calabria move SE-ward toward the Ionian Sea at 3–5 mm/yr, marking a change across the Messina Straits.

We use horizontal GPS velocities in eastern Sicily and western Calabria to compute the velocity gradient field over a regular grid (Fig. 3 and Fig. S5), while taking into account the stations distribution and velocity uncertainties. We find that local features of the strain rate field are well determined in the Central Aeolian Is. and across the Messina Straits (Fig. 4). Here we observe a rapid transition from fast N–S to NNE–SSW oriented shortening (at rates of ~240 nanostrains/yr), across the Salina–Lipari–Vulcano lineament, to slower NW–SE oriented extension (at rates of ~65 nanostrains/yr) across the Messina Straits. While fast shortening in the Central Aeolian region may be related to the complex interplay between plate convergence and volcano-tectonic processes, and fast rotation rates suggest the presence of an important kinematic discontinuity, extensional deformation across the Straits is in agreement with other stress indicators and active faulting data. Our results differ from those presented in Mattia et al. (2009), who found faster deformation rates (~150 nanostrains/yr) and a highly variable orientation of the principal strain rate axes in the Peloritani and Messina Straits area. However, the spatial scale at which those changes occur is less than the spacing of the GPS stations, suggesting that the variability found by Mattia et al. (2009) is likely due to the model approach, rather than being a real tectonic signal.

Assuming that the observed velocity gradient across the Messina Straits (Fig. 5) is due to slip on a single planar dislocation locked above a certain depth and that all strain that accumulates interseismically is elastic, we develop a simple dislocation model of the deformation. We use a non-linear constrained optimization algorithm to invert for the fault locking depth, dip, upper-edge location and slip-rate, constraining the fault strike to be normal to the estimated extensional deformation. We find that the observed velocity gradient can be explained by $-3.5^{-1.3}_{+2.0}$ mm/yr dip–slip-rate on a SE-ward $30.1^{-0.7}_{+1.1}°$ dipping normal fault, with $1.6^{-0.2}_{+0.3}$ mm/yr of right-lateral slip component, locked at $7.6^{-2.9}_{+4.6}$ km depth. Uncertainties associated with the modeled fault plane geometry and slip-rates have been evaluated adopting a bootstrap approach (Fig. 6). The analysis shows that the dip direction and dip angle are quite well determined by the data, whereas, error bounds on the locking depth and the fault edge position are larger. Adding new CGPS stations across the Straits and improving catalogues of relocated seismicity will certainly help in reducing such uncertainties.

The results of our local dislocation analysis provide some clues about the geometry and kinematics of the fault responsible for the 1908 Messina–Reggio Calabria earthquake. The continuation of the modeled fault plane (see Fig. 5) in the upper 7–8 km agrees rather well with the NE–SW oriented gently SE-ward dipping fault plane proposed by several authors as the fault segment that ruptured during the Messina earthquake (see Pino et al., 2009 for a summary). The analysis of leveling and seismological data suggests that the 1908 earthquake ruptured a ~40 km long segment with a predominant normal slip component, although a significant right-lateral slip component has been suggested by some authors (e.g., Amoruso et al. 2002). Recently, Argnani et al. (2009), carried out a marine multichannel seismic survey in the area of the Messina 1908 earthquake, and found great structural complexity within the Messina Straits, with the best imaged fault occurring offshore southern Calabria. This fault strikes NW–SE, and is not compatible with the NW–SE extensional deformation and fault model imaged by our GPS data. Difficulties in detecting the 1908 earthquake causative fault from geophysical prospecting in the Messina Straits point to a possibly blind seismogenic fault. Valensise and Pantosti (1992), in fact, proposed that repeated 1908-type earthquakes occurring on a blind normal fault, with similar dislocation along similar fault length, have largely shaped the present structure of the Messina Straits, and recent compilations of geological and tectonic data (http://diss.rm.ingv.it/diss/) suggest a long-term geological slip-rate of 1–2 mm/yr, which is consistent with the interseismic slip-rate derived in our analysis. The discrepancy, in fact, stands still within the 95% confidence bounds provided by our bootstrap analysis of model uncertainties (Table 1).

In order to frame the observed local deformation features within the present-day microplate kinematics, we use an elastic block-modeling approach that, taking into account both crustal blocks rotations and elastic strains at block-bounding faults, allows to investigate the impact of elastic strain contributes from other nearby active faults onto the velocity gradient measured across the Messina Straits. We develop a block geometry allowing the Tyrrhenian, Sicily and NE-Sicily, Calabria, and Apulia blocks to move independently, or partially independently, with respect to a fixed Ionian block that is moving either with the Nubian or Apulian plate. Using Nubia-fixed or Apulia-fixed velocities (Fig. 7) allows us to account for both end-members kinematics along the Sicily–Calabria plate boundary (e.g., D'Agostino et al., 2008; Serpelloni et al., 2007). Both models match the horizontal velocity data quite well (Fig. S5), and suggest that the elastic contribution of the Tindari–Giardini Fault system and the western Calabria normal fault system on the inverted slip-rates of the Messina Straits Fault, is minimal or negligible (Fig. 8). In contrast, both models predict elastic strain accumulation on the subduction interface, offshore Calabria, and show that the inferred slip-rates on the Messina Fault are strongly impacted by the assumed locking width of the Calabrian subduction thrust, increasing the uncertainties of fault slip-rates estimated from geodetic data.

Evaluating the interseismic Messina Fault slip-rate is certainly a fundamental task for estimating the seismic hazard of this area. Our analysis confirms that the Messina Straits is undergoing NW–SE extension of ~3 mm/yr and that the surface deformation is consistent with a gently SE-ward dipping normal fault, with a slip-rate comparable (within the model uncertainties) to that estimated from geological data. However, the estimate of geodetic fault slip-rates in the Sicily and Calabria area is challenged by the tectonic and kinematic complexity of this segment of the Africa–Eurasia plate boundary. In particular, the possible accumulation of substantial elastic strain at the subduction thrust, which could be released in future large earthquakes, requires further data and investigation.

Acknowledgements

This work was partially supported by the SIGRIS project, funded by the Italian Space Agency (ASI), and benefited from funding provided by the Italian Presidenza del Consiglio dei Ministri, Dipartimento della Protezione Civile (projects DPC-S5 and DPC-S1). We are thankful to all individuals and institutions contributing in the GPS data, particularly to all INGV staff involved in the development of the RING network, and to SOPAC, UNAVCO and the Calabrian Arc and CATSCAN projects.

We thank the GAMIT/GLOBK MIT group and Danan Dong for help and support on GPS data processing and post-processing, and Brendan Meade for making his block-modeling code available. We thank Luca Valensise and Andrea Argnani for their comments on an early draft of the manuscript. The Editor, Rob van der Hilst, Rob Govers and an anonymous reviewer greatly improved the quality of the manuscript. Some of the figures have been created using the Generic Mapping Tools (GMT) software (Wessel and Smith, 1998).

Appendix A. Supplementary data

Supplementary data associated with this article can be found, in the online version, at doi: 10.1016/j.epsl.2010.08.005.

References

Altamimi, Z., Collilieux, X., Legrand, J., Garayt, B., Boucher, C., 2007. ITRF2005: a new release of the International Terrestrial Reference Frame based on time series of station positions and earth orientation parameters. J. Geophys. Res. 112, B09401. doi:10.1029/2007JB004949.

Amoruso, A., Crescentini, L., Scarpa, R., 2002. Source parameters of the 1908 Messina Straits, Italy, earthquake from geodetic and seismic data. J. Geophys. Res. 107 (B4), 2080. doi:10.1029/2001JB000434.

Anzidei, M., Baldi, P., Bonini, C., Casula, G., Gandolfi, S., Riguzzi, F., 1998. Geodetic surveys across the Messina Straits (southern Italy) seismogenetic area. J. Geodyn. 25, 85–97.

Anzidei, M., Baldi, P., Casula, G., Galvani, A., Mantovani, E., Pesci, A., Riguzzi, F., Serpelloni, E., 2001. Insights into present-day crustal motion in the central Mediterranean area from GPS surveys. Geophys. J. Int. 146, 98–110.

Argnani, A., 2009. Evolution of the southern Tyrrhenian slab tear and active tectonics along the western edge of the Tyrrhenian subducted slab. Geol. Soc., London, Spec. Publ. 311, 193–212.

Argnani, A., Bonazzi, C., 2005. Malta Escarpment fault zone offshore eastern Sicily: Pliocene–Quaternary tectonic evolution based on new multichannel seismic data. Tectonics 24 (TC4009). doi:10.1029/2004TC001656.

Argnani, A., Serpelloni, E., Bonazzi, C., 2007. Pattern of deformation around the central Aeolian Islands: evidence from multichannel seismics and GPS data. Terra Nova 19, 317–323.Argus, D.F., Gordon, R.G., Demets, C., Stein, S., 1989. Closure of the Africa Eurasia North America Plate motion circuit and tectonics of the Gloria Fault. J. Geophys. Res. 94, 5585–5602.

Argnani, A., Brancolini, G., Bonazzi, C., Rovere, M., Accaino, F., Zgur, F., Lodolo, E., 2009. The results of the Taormina 2006 seismic survey: possible implications for active tectonics in the Messina Straits. Tectonophys 476 (1–2), 159–169.

Arnadottir, T., Segall, P., 1994. The 1989 Loma–Prieta earthquake imaged from inversion of geodetic data. J. Geophys. Res. 99, 21835–21855.

Avallone, A., Selvaggi, G., D'Anastasio, E., D'Agostino, N., Pietrantonio, G., Riguzzi, F., Serpelloni, E., Anzidei, M., Casula, G., Cecere, G., D'Ambrosio, C., De Martino, P., Devoti, R., Falco, L., Mattia, M., Rossi, M., Obrizzo, F., Tammaro, U., Zarrilli, L., 2010. The RING network: improvement of a GPS velocity field in the central Mediterranean. Ann. Geophy. 53, 2. doi:10.4401/ag-4549.

Basili, R., Valensise, G., Vannoli, P., Burrato, P., Fracassi, U., Mariano, S., Tiberti, M., Boschi, E., 2008. The Database of Individual Seismogenic Sources (DISS), version 3: summarizing 20 years of research on Italy's earthquake geology. Tectonophysics 453, 20–43.

Beavan, J., Tregoning, P., Bevis, M., Kato, T., Meertens, C., 2002. Motion and rigidity of the Pacific Plate and implications for plate boundary deformation. J. Geophys. Res. 107. doi:10.1029/2001JB000282.

Bencini, P., 1975. Geodetic measurements made by Istituto Geografico Militare in the Strait of Messina area. Tectonophysics 29, 331–337.

Billi, A., Barberi, G., Faccenna, C., Neri, G., Pepe, F., Sulli, A., 2006. Tectonics and seismicity of the Tindari Fault System, southern Italy: crustal deformations at the transition between ongoing contractional and extensional domains located above the edge of a subducting slab. Tectonics 25 (TC2006). doi:10.1029/2004TC001763.

Blewitt, G., Lavallee, D., 2002. Effect of annual signals on geodetic velocity. J. Geophys. Res. 107 (B7), 2145. doi:10.1029/2001JB000570.

Bonforte, A., Puglisi, G., 2006. Dynamics of the eastern flank of Mt. Etna volcano (Italy) investigated by a dense GPS network. J. Volcanol. Geoth. Res. 153 (3–4), 357–369.

Boschi, E., Pantosti, D., Valensise, G., 1989. Modello di sorgente per il terremoto di Messina del 1908 ed evoluzione recente dell'area dello Stretto. G.N.G.T.S, pp. 245–258. Rome.

Boschi, E., Guidoboni, M., Ferrari, G., Mariotti, G., Valensise, G., Gasperini, P., 2000. Catalogue of strong Italian earthquakes, 461 B.C. to 1997. Ann. Geofis. 43, 609–868.

Bottari, A., Capuano, P., Denatale, G., Gasparini, P., Neri, G., Pingue, F., Scarpa, R., 1989. Source parameters of earthquakes in the Strait of Messina, Italy, during this century. Tectonophysics 166, 221–234.

Burgmann, R., Segall, P., Lisowski, M., Svarc, J., 1997. Postseismic strain following the 1989 Loma Prieta earthquake from GPS and leveling measurements. J. Geophys. Res. 102, 4933–4955.

Caputo, M., Pieri, L., Barbarella, M., Gubellini, A., Russo, P., Console, R., 1981. Geophysical and geodetic observations in the Messina Straits. Tectonophysics 74, 147–154.

Carminati, E., Wortel, M.J.R., Spakman, W., Sabadini, R., 1998. The role of slab detachment processes in the opening of the western-central Mediterranean basins: some geological and geophysical evidence. Earth Planet. Sci. Lett. 160 (3–4), 651–665.

Cernobori, L., Hirn, A., McBride, J.H., Nicolich, R., Petronio, L., Romanelli, M., 1996. Crustal image of the Ionian basin and its Calabrian margins. Tectonophysics 264, 175–189.

Chiarabba, C., Jovane, L., DiStefano, R., 2005. A new view of Italian seismicity using 20 years of instrumental recordings. Tectonophysics 395, 251–268.

Cifelli, F., Mattei, M., Della Seta, M., 2008. Calabrian Arc oroclinal bending: the role of subduction. Tectonics 27 (5). doi:10.1029/2008TC002272.

D'Agostino, N., Selvaggi, G., 2004. Crustal motion along the Eurasia–Nubia plate boundary in the Calabrian Arc and Sicily and active extension in the Messina Straits from GPS measurements. J. Geophys. Res. 109, B11402. doi:10.1029/2004JB002998.

D'Agostino, N., Avallone, A., Cheloni, D., D'Anastasio, E., Mantenuto, S., Selvaggi, G., 2008. Active tectonics of the Adriatic region from GPS and earthquake slip vectors. J. Geophys. Res. 113, B12413. doi:10.1029/2008JB005860.

Devoti, R., Riguzzi, F., Cuffaro, M., Doglioni, C., 2008. New GPS constraints on the kinematics of the Apennines subduction. Earth Planet. Sci. Lett. 273, 163–174.

Dewey, J.F., Pitman, W.C., Ryan, W.B.F., Bonnin, J., 1973. Plate tectonics and evolution of Alpine system. Geol. Soc. Am. Bull. 84, 3137–3180.

Dixon, T.H., Miller, M., Farina, F., Wang, H.Z., Johnson, D., 2000. Present-day motion of the Sierra Nevada block and some tectonic implications for the Basin and Range province, North American Cordillera. Tectonics 19, 1–24.

Doglioni, C., 1991. A proposal for the kinematic modeling of W-dipping subductions—possible applications to the Tyrrhenian Apennines system. Terra Nova 3 (4), 423–434.

Dong, D., Herring, T.A., King, R.W., 1998. Estimating regional deformation from a combination of space and terrestrial geodetic data. J. Geodesy. 72, 200–214.

Dong, D., Fang, P., Bock, Y., Cheng, M.K., Miyazaki, S., 2002. Anatomy of apparent seasonal variations from GPS-derived site psosition time series. J. Geophys. Res. 107 (B4), 2075. doi:10.1029/2001JB000573.

Faccenna, C., Becker, T.W., 2010. Shaping mobile belts by small-scale convection. Nature 465 (7298), 602–605.

Faccenna, C., Becker, T.W., Lucente, F.P., Jolivet, L., Rossetti, F., 2001. History of subduction and back-arc extension in the Central Mediterranean. Geophys. J. Int. 145, 809–820.

Faccenna, C., Piromallo, C., Crespo-Blanc, A., Jolivet, L., Rossetti, F., 2004. Tectonics 23 (TC1012). doi:10.1029/2002TC001488.

Ferranti, L., Monaco, C., Antonioli, F., Maschio, L., Kershaw, S., Verrubbi, V., 2007. The contribution of regional uplift and coseismic slip to the vertical crustal motion in the Messina Straits, southern Italy: evidence from raised Late Holocene shorelines. J. Geophys. Res. 112, B06401. doi:10.1029/2006JB004473.

Ghisetti, F., 1984. Recent deformations and the seismogenic source in the Messina Strait (Southern Italy). Tectonophysics 109, 191–208.

Goes, S., Giardini, D., Jenny, S., Hollenstein, C., Kahle, H.G., Geiger, A., 2004. A recent tectonic reorganization in the south-central Mediterranean. Earth Planet. Sci. Lett. 226, 335–345.

Govers, R., Wortel, M.J.R., 2005. Lithosphere tearing at STEP faults: response to edges of subduction zones. Earth Planet. Sci. Lett. 236, 505–523.

Gueguen, E., Doglioni, C., Fernandez, M., 1998. On the post-25 Ma geodynamic evolution of the western Mediterranean. Tectonophysics 298, 259–269.

Gutscher, M.A., Roger, J., Baptista, M.A., Miranda, J.M., Tinti, S., 2006. Source of the 1693 Catania earthquake and tsunami (southern Italy): new evidence from tsunami modeling of a locked subduction fault plane. Geophys. Res. Lett. 33, L08309. doi:10.1029/2005GL025442.

Hammond, W.C., Thatcher, W., 2004. Contemporary tectonic deformation of the Basin and Range province, western United States: 10 years of observation with the Global Positioning System. J. Geophys. Res. 109, B08403. doi:10.1029/2003JB002746.

Herring, T., King, R.W., McClusky, S., 2006. GAMIT Reference Manual, Release 10.3, Department of Earth, Atmospheric, and Planetary Sciences. Massachussetts Institute of Technology.

Hollenstein, C., Kahle, H.G., Geiger, A., Jenny, S., Goes, S., Giardini, D., 2003. New GPS constraints on the Africa–Eurasia plate boundary zone in southern Italy. Geophys. Res. Lett. 30 (18), 1935. doi:10.1029/2003GL017554.

Jenny, S., Goes, S., Giardini, D., Kahle, H.G., 2004. Earthquake recurrence parameters from seismic and geodetic strain rates in the eastern Mediterranean. Geophys. J. Int. 157, 1331–1347.

Langbein, J., Johnson, H., 1997. Correlated errors in geodetic time series: implications for time-dependent deformation. J. Geophys. Res. 102, 591–603.

Lucente, F.P., Margheriti, L., Piromallo, C., Barruol, G., 2006. Seismic anisotropy reveals the long route of the slab through the western-central Mediterranean mantle. Earth Planet. Sci. Lett. 241, 517–529.

Lundgren, P., Casu, F., Manzo, M., Pepe, A., Berardino, P., Sansosti, E., Lanari, R., 2004. Gravity and magma induced spreading of Mount Etna volcano revealed by satellite radar interferometry. Geophys. Res. Lett. 31 (4). doi:10.1029/2003GL018736.

Malinverno, A., Ryan, W.B.F., 1986. Extension in the Tyrrhenian Sea and shortening in the Apennines as result of arc migration driven by sinking of the lithosphere. Tectonics 5, 227–245.

Margheriti, L., 2008. Understanding crust dynamics and subduction in southern Italy. Eos Trans. AGU 89.

Matsu'ura, M., Sato, T., 1989. A dislocation model for the earthquake cycle at convergent plate boundaries. Geophys. J. Int. 96 (1), 23–32.

Mattia, M., Palano, M., Bruno, V., Cannavò, F., Bonaccorso, A., Gresta, S., 2008. Tectonic features of the Lipari–Vulcano complex (Aeolian archipelago, Italy) from 10 years (1996–2006) of GPS data. Terra Nova 20 (5), 370–377.

Mattia, M., Palano, M., Bruno, V., Bruno, V., Cannavò, F., 2009. Crustal motion along the Calabro–Peloritano Arc as imaged by twelve years of measurements on a dense GPS network. Tectonophys 476 (3–4), 528–537.

Meade, B.J., Hager, B.H., 2005. Block models of crustal motion in southern California constrained by GPS measurements. J. Geophys. Res. 110, B03403. doi:10.1029/2004JB003209.
Mele, G., 1998. High-frequency wave propagation from mantle earthquakes in the Tyrrhenian Sea: new constraints for the geometry of the south Tyrrhenian subduction zone. Geophys. Res. Lett. 25, 2877–2880.
Meletti, C., Galadini, F., Valensise, G., Stucchi, M., Basili, R., Barba, S., Vannucci, G., Boschi, E., 2008. A seismic source zone model for the seismic hazard assessment of the Italian territory. Tectonophysics 450, 85–108.
Monaco, C., Tortorici, L., 2000. Active faulting in the Calabrian arc and eastern Sicily. J. Geodyn. 29, 407–424.
Musumeci, C., Patane, D., Scarfi, L., Gresta, S., 2005. Stress directions and shear-wave anisotropy: observations from local earthquakes in southeastern Sicily, Italy. B. Seismol. Soc. Am. 95, 1359–1374.
Neri, G., Barberi, G., Orecchio, B., Mostaccio, A., 2003. Seismic strain and seismogenic stress regimes in the crust of the southern Tyrrhenian region. Earth Planet. Sci. Lett. 213, 97–112.
Nicolosi, I., Speranza, F., Chiappini, M., 2006. Ultrafast oceanic spreading of the Marsili Basin, southern Tyrrhenian Sea: evidence from magnetic anomaly analysis. Geology 34, 717–720.
Okada, Y., 1985. Surface deformation due to shear and tensile faults in a half-space. B. Seismol. Soc. Am. 75, 1135–1154.
Pepe, F., Sulli, A., Bertotti, G., Catalano, R., 2005. Structural highs formation and their relationship to sedimentary basins in the north Sicily continental margin (southern Tyrrhenian Sea): implication for the Drepano Thrust Front. Tectonophys 409, 1–18.
Pino, N.A., Piatanesi, A., Valensise, G., Boschi, E., 2009. The 28 December 1908 Messina Straits earthquake (M(w)7.1): a great earthquake throughout a century of seismology. Seismol. Res. Lett. 80, 243–259.
Piromallo, C., Morelli, A., 2003. P wave tomography of the mantle under the Alpine–Mediterranean area. J. Geophys. Res. 108 (B2), 2065. doi:10.1029/2002JB001757.
Pondrelli, S., Piromallo, C., Serpelloni, E., 2004. Convergence vs. retreat in Southern Tyrrhenian Sea: insights from kinematics. Geophys. Res. Lett. 31, L06611. doi:10.1029/2003GL019223.
Rosenbaum, G., Lister, G.S., Duboz, C., 2002. Relative motions of Africa, Iberia and Europe during Alpine orogeny. Tectonophysics 359, 117–129.
Royden, L.H., 1993. Evolution of retreating subduction boundaries formed during continental collision. Tectonics 12 (3), 629–638.
Savage, J.C., Burford, R.O., 1970. Accumulation of tectonic strain in California. B. Seismol. Soc. Am. 60, 1877–1896.
Serpelloni, E., Anzidei, M., Baldi, P., Casula, G., Galvani, A., 2005. Crustal velocity and strain-rate fields in Italy and surrounding regions: new results from the analysis of permanent and non-permanent GPS networks. Geophys. J. Int. 161, 861–880.
Serpelloni, E., Casula, G., Galvani, A., Anzidei, M., Baldi, P., 2006. Data analysis of permanent GPS networks in Italy and surrounding regions: application of a distributed processing approach. Ann. Geophys.-Italy 49, 897–928.
Serpelloni, E., Vannucci, G., Pondrelli, S., Argnani, A., Casula, G., Anzidei, M., Baldi, P., Gasperini, P., 2007. Kinematics of the Western Africa–Eurasia plate boundary from focal mechanisms and GPS data. Geophys. J. Int. 169, 1180–1200.
Shen, Z.K., Jackson, D., Ge, B.X., 1996. Crustal deformation across and beyond the Los Angeles basin from geodetic measurements. J. Geophys. Res. 101 (B12), 27957–27980.
Shen, Z.-K., Jackson, D.D., Kagan, Y.Y., 2007. Implications of geodetic strain rate for future earthquakes, with a five-year forecast of M5 earthquakes in Southern California. Seismol. Res. Lett. 78, 116–120.
Valensise, G., Pantosti, D., 1992. A 125 Kyr-long geological record of seismic source repeatability— the Messina Straits (Southern Italy) and the 1908 Earthquake (M(S) 7 1–2). Terra Nova 4, 472–483.
Wessel, P., Smith, W.H.F., 1998. New, improved version of the Generic Mapping Tools released. Eos Trans. AGU 79, 579.
Westaway, R., 1993. Quaternary uplift of Southern Italy. J. Geophys. Res. 98, 21741–21772.
Williams, S.D.P., 2003. The effect of coloured noise on the uncertainties of rates estimated from geodetic time series. J. Geodesy. 76, 483–494.
Williams, S.D.P., Bock, Y., Fang, P., Jamason, P., Nikolaidis, R.M., Prawirodirdjo, L., Miller, M., Johnson, D.J., 2004. Error analysis of continuous GPS position time series. J. Geophys. Res. 109, B03412. doi:10.1029/2003JB002741.
Wortel, M.J.R., Spakman, W., 2000. Subduction and slab detachment in the Mediterranean–Carpathian region. Science 290 (5498), 1910–1917.